PCCP

Accepted Manuscript

ROYAL SOCIETY OF CHEMISTRY

www.rsc.org/pccp

Effects of thermodynamic inhibitors on the dissociation of methane hydrate: A molecular dynamics study

Takuma Yagasaki,[†] Masakazu Matsumoto[†] and Hideki Tanaka[†, ‡, *]

[†]Department of Chemistry, Faculty of Science, Okayama University, Okayama, 700-8530, Japan

[‡]Research Center of New Functional Materials for Energy Production, Storage and Transport, Okayama, 700-8530, Japan

[*]Email: htanakaa@okayama-u.ac.jp.

Table of contents entry

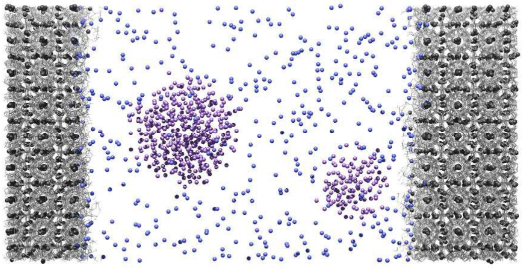

Bubble formation and the hydration free energy of methane play important roles in the hydrate dissociation. The effects of methanol and NaCl on them are investigated using molecular dynamics simulations.

Abstract

We investigate the effects of methanol and NaCl, which are known as thermodynamics inhibitors of hydrate, on the dissociation kinetics of methane hydrate in aqueous solutions by using molecular dynamics simulations. It is shown that the dissociation rate is not a constant but changes with time. The dissociation rate in the initial stage is increased by methanol whereas it is decreased by NaCl. This difference arises from the opposite effects of the two thermodynamic inhibitors on the hydration free energy of methane. The dissociation rate of methane hydrate is increased by formation of methane bubbles in the aqueous phase because the bubbles absorb surrounding methane molecules. It is found that both methanol and NaCl facilitate the bubble formation. However, their mechanisms are completely different from each other. The presence of ions enhances the hydrophobic interactions between methane molecules. In addition, the ions in the solution cause a highly non-uniform distribution of dissolved methane molecules. These two effects result in the easy formation of bubbles in the NaCl solution. In contrast, methanol assists the bubble formation because of its amphiphilic character.

Introduction

Clathrate hydrates are crystalline solids, individual water cages of which encapsulate one or more guest molecules.[1] A water molecule in a clathrate hydrate has four hydrogen bonds with neighboring water molecules and thus its local structure is similar to a water molecule in ice. It is known that many molecular species, that are small and mostly hydrophobic, form clathrate hydrates. Clathrate hydrates that occur in nature are either structure I or II in most cases (Figure 1). A unit cell of structure I clathrate hydrate consists of two 5^{12} and six $5^{12}6^{2}$ water cages and that of structure II is composed of sixteen 5^{12} and eight $5^{12}6^{4}$ cages. Due to the presence of large $5^{12}6^{4}$ cages, relatively large molecules such as propane form structure II hydrate. Very small molecules like neon also form structure II hydrate because of the large number of 5^{12} cages. Molecules of intermediate size such as methane form structure I hydrate.

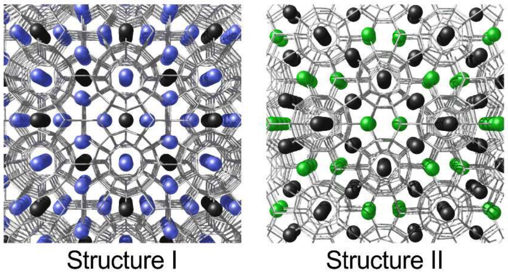

Figure 1. Structure I and structure II clathrate hydrates. The hydrogen bond network of water is represented by gray lines. Guest molecules in 5^{12}, $5^{12}6^{2}$, and $5^{12}6^{4}$ cages are shown by black, blue and green spheres, respectively.

It is important to understand molecular mechanism of hydrate dissociation. There is a huge amount of natural gas hydrates in ocean sediments, and they are expected as a future energy resource.[1-4] A practical method to recover natural gas from ocean methane hydrate is the depressurization method.[1] In this method, methane hydrate is dissociated by reduction of pressure in the hydrate-bearing layer, and the efficiency of the methane production depends on the rate of hydrate dissociation. It is known that clathrate hydrates form in gas and oil pipelines.[1, 5, 6] This is a serious industrial problem because the pipeline must be shut down until the hydrate plugs are removed. Elucidation of the dissociation process of gas hydrates is important for the pipeline plug remediation. The hydrate dissociation is an important process also in gas separation and storage using clathrate hydrates.[3, 7-12]

Molecular dynamics (MD) and Monte Carlo (MC) simulations have provided a wealth of microscopic information on clathrate hydrates.[13] Early simulation studies have focused on, for example, thermodynamic stability,[14-25] structure,[26-31] formation,[32-67] molecular diffusion,[68-73] and thermal conductivity.[74, 75] The dissociation process of gas hydrates has also been extensively studied.[76-95] The dissociation rate of gas hydrates largely depends on mass and heat transfer. The rate which is in the absence of mass and heat transfer is important to understand intrinsic kinetics, and it is required for construction of kinetics models of gas hydrates.[1, 96, 97] MD simulations are useful to evaluate the intrinsic kinetics because the concentration of molecules in a local region can be monitored on a molecular scale and the effect of heat transfer can be eliminated by using a strong coupling between the system and a thermal reservoir.

It is possible to alter the dissociation temperature of gas hydrates by using additives called thermodynamic inhibitors (TIs) such as alcohols, glycols and salts.[1] TIs are used to prohibit formation of hydrates in pipelines and help the plug remediation. Methanol is the most common TI because of its low cost. At a temperature higher than the ice point, the final state of the dissociation process of a crystalline methane hydrate is the two-phase equilibrium of methane gas and liquid water. The molar free energy of the hydrate crystal is equivalent to that of the two-phase equilibrium state at the dissociation temperature. The lowering of the dissociation temperature due to TIs arises from the decrease in the chemical potential of water in the liquid phase.

In general, the dissociation rate of a solid is dominated by the difference in the free energy between the initial and final states.[98] The dissociation of methane hydrate in water is not the case because there is an intermediate metastable state between the initial and final states, i.e., the aqueous solution of methane without the gas phase. We showed that the dissociation rate depends also on the free energy of the intermediate in a previous paper.[93] TIs lower the free energy of the final state but it is not certain whether they also lower the free energy of the intermediate state. If a TI destabilizes the intermediate state, the TI decreases the dissociation rate although it lowers the dissociation temperature.

There are two types of TIs, i.e., salts and amphiphilic molecules.[1] In a previous paper, we demonstrated the significant effects of NaCl on the hydrate dissociation.[94] A question raised here is how amphiphilic inhibitors affect the dissociation kinetics. In this paper, we compare the dissociation behaviors of methane hydrate in pure water, in an aqueous NaCl solution, and in a methanol solution using MD simulations. We first discuss the dissociation mechanism of methane hydrate in pure water from a somewhat different perspective than the previous papers.[93, 94] Then, the dissociation behaviors in NaCl and methanol solutions are examined. We demonstrate that the effects of the two TIs on the dissociation mechanism are largely different from each other. The difference is discussed in terms of the free energies of states emerging in the dissociation process.

Computational details

We perform MD simulations of the dissociation of methane hydrate in pure water, in an aqueous methanol solution, and in an aqueous NaCl solution. All systems consist of an aqueous solution and a slab of structure I hydrate in which all the cages are filled with methane. The pure water system contains 3776 methane and 53248 water molecules. The size of the simulation cell is roughly $95 \times 95 \times 190$ $Å^3$. The initial configuration is shown in Figure 2a. The hydrate slab occupies roughly half of the system. The methanol solution system comprises 3776 methane, 47104 water, and 2560 methanol molecules, respectively. The mole fraction of methanol in the aqueous phase is approximately 0.1, which corresponds to ~15 wt %. The number of NaCl, methane, and water molecules in the NaCl solution system are 1961, 3776, and 49326. The concentration of NaCl in the aqueous phase is 4.8 mol kg^{-1} in the initial configuration.

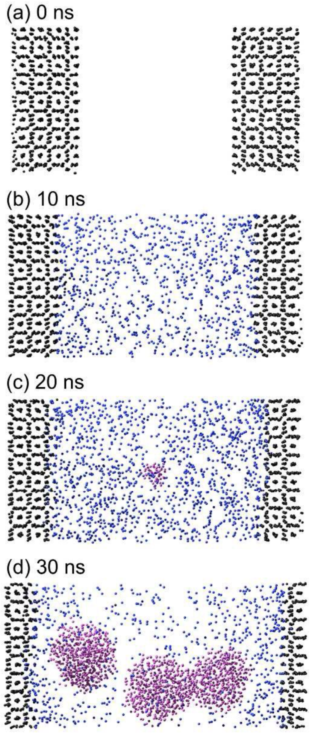

Figure 2 Snapshots along the dissociation process of methane hydrate in pure water at *T* = 312 K. Black, blue, and purple particles are methane molecules in the hydrate slab, those dissolved in the aqueous phase, and those in bubbles, respectively. Water molecules are not shown.

MD simulations are performed with the GROMACS 4.6 package.[99, 100] Long-range coulomb interactions are treated with the particle mesh Ewald method.[101, 102] The TIP4P/2005 model is employed for water.[103] The interaction parameters for methane and methanol are taken from the OPLS united atom force field.[104, 105] The parameters for Na^+ and Cl^- are taken from ref. 106. The pressure is kept with the semi-isotropic Parrinello-Rahman scheme which allows the box length in the *z*-direction to change independently from those of the *x*- and *y*-directions.[107, 108] The temperature is maintained by the Nose-Hoover thermostat.[109, 110]

We first equilibrate the aqueous phase at 300 K for 1 ns with fixing the configurations of the hydrate phase. Next, in order to relax the structure of the hydrate, a MD simulation is performed for 80 ps at $T = 100$ K and $P = 1$ bar without constraints. Then, the temperature is sharply raised to a target value keeping the pressure at 1 bar. This instant is referred to as the time origin, $t = 0$.

During the dissociation process, methane molecules are released from the hydrate slab, and they form bubbles when the concentration of methane reaches the limit of supersaturation. We classify methane molecules into three types, molecules in the hydrate slab, those dissolved in the aqueous phase, and those in bubbles. First, the F_3 tetrahedrality parameter[76] is evaluated for water molecules in the first solvation shell ($r < 5.5$ Å) of methane. Then, the number of water molecules with a highly tetrahedral structure ($F_3 < 0.3$) is counted for each methane molecule. If this number is more than 15, the methane molecule is assumed to be in a hydrate cage. The remaining methane molecules are further classified into two types based on a cluster analysis. We define that two methane molecules are “connected” when the distance between them is shorter than 6 Å, which is the first minimum of the methane-methane radial distribution function in the aqueous phase. We observe that the maximum cluster consists of roughly 30 molecules before a cluster rapidly grows in the aqueous phase. Therefore, we define a cluster of methane molecules as a bubble if the number of methane molecules in the cluster is more than 30. Isolated methane molecules and methane molecules in clusters smaller than the threshold are defined as those dissolved in the aqueous phase. Figure 2 demonstrates that methane molecules are well classified with these criteria.

In addition to the MD simulations of the non-equilibrium hydrate dissociation process, we perform equilibrium MD simulations of a methane molecule dissolved in aqueous solutions in order to evaluate the hydration free energy of methane. The aqueous solution consists of 1000 water molecules for the pure water system, 100 methanol and 900 water molecules for the methanol solution system, and 74 NaCl and 852 water molecules for the NaCl solution system. The potential energy of the system is described by

$$V_\lambda = V_{vv} + \lambda \sum_{i=1}^{N_v} \left(4\varepsilon_{iu} \left\{ \left(\frac{\sigma_{iu}}{r'_{iu}(\lambda)} \right)^{12} - \left(\frac{\sigma_{iu}}{r'_{iu}(\lambda)} \right)^{6} \right\} \right), \tag{1}$$

where V_{vv} is the sum of the solvent-solvent interactions, N_v is the total number of the interactions sites on solvent molecules, and σ_{iu} and ε_{iu} are the Lennard-Jones (LJ) parameters for the solvent-solute interactions. The λ-dependent distance is given by

$$r'_{iu}(\lambda) = \left\{ 0.5\sigma_{iu}^6 (1-\lambda) + r_{iu}^6 \right\}^{\frac{1}{6}}. \tag{2}$$

This expression for the potential function, called the soft-core form, is required to avoid large fluctuations near $\lambda = 0$ in the free energy calculation.[111] The hydration free energy, i.e., the free energy difference between $\lambda = 1$ and 0, is given by

$$G_{hyd} = \sum_{i=0}^{N_\lambda - 1} \left\{ G(\lambda_{i+1}) - G(\lambda_i) \right\} \tag{3}$$

with

$$\lambda_i = \frac{i}{N_\lambda}. \tag{4}$$

The number of states N_λ is set to 20. The simulation is performed for 2 ns at each state. The free energy difference between adjacent states is calculated from the acceptance ratio method:[112]

$$G(\lambda_{i+1}) - G(\lambda_i) = \frac{C}{\beta} \tag{5}$$

with

$$\left\langle \frac{1}{1+\exp\left(\beta V_{\lambda_{i+1}} - \beta V_{\lambda_i} - C\right)} \right\rangle_{\lambda_i} = \left\langle \frac{1}{1+\exp\left(\beta V_{\lambda_i} - \beta V_{\lambda_{i+1}} + C\right)} \right\rangle_{\lambda_{i+1}} \tag{6}$$

where β is the reciprocal temperature and $\langle \ \rangle_{\lambda_i}$ represents the ensemble average obtained with the potential V_{λ_i}.

Results and Discussion

Dissociation of methane hydrate in pure water

Figure 3 presents the time evolution of the number of methane molecules in the hydrate slab, N_h, in pure water. We observe a sharp drop of N_h from ~500 to 0 in the last stage of the dissociation process. This drop is due to the rapid collapse of a thin solid slab, and it is commonly observed in MD simulations of ice and clathrate hydrates.[58, 84, 113] The negative slope in N_h, ($-dN_h/dt$), can be assumed as the rate of dissociation because the surface area of the hydrate does not change with time owing to the slab geometry. Figure 3a demonstrates that N_h linearly decreases with time except for the final collapse for $T \geq 320$ K. This indicates that the dissociation rate is a constant with respect to time in this high temperature region. In contrast, as shown in Figure 3b, the slope changes with time at lower temperatures.[93] At $T = 312$ K, for example, the dissociation rate initially decreases with time, and then it turns to increase at $t \sim 20$ ns. This trend is seen more clearly at $T = 308$ and 304 K.

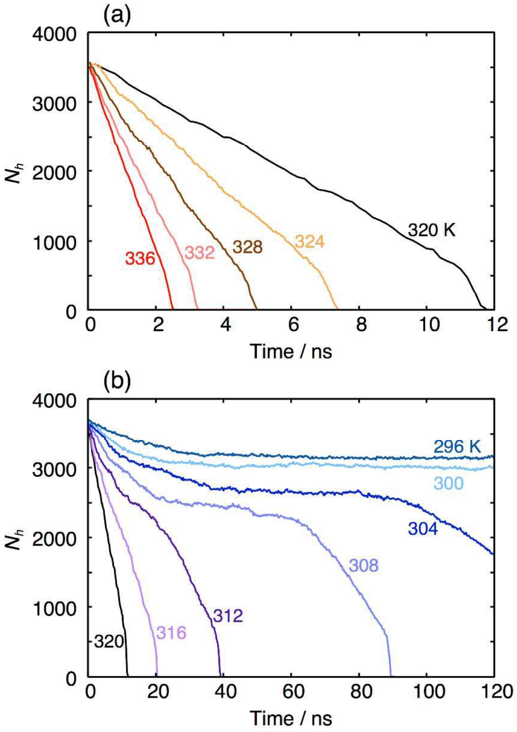

Figure 3 Time evolution of the number of methane molecules in the hydrate slab, N_h, for the pure water system at (a) high and (b) low temperatures.

In Figure 4b, we plot the number of methane molecules dissolved in the aqueous solution, N_a, at T = 312 K. Because methane molecules are released from the hydrate slab, N_a increases with time for $0 < t < 20$ ns. The concentration of methane in the aqueous solution reaches the limit of supersaturation at t = 20 ns, and the first bubble of methane form in the solution as shown in Figure 2c. The second and third bubbles emerge at t = 20.8 and 21.2 ns, respectively. The number of methane molecules in the bubbles, N_b, rapidly increases whereas N_a decreases because the bubbles absorb methane molecules from the aqueous solution. The change in the slope of N_h shows that the dissociation rate increases after the formation of bubbles at $t \sim 20$ ns.

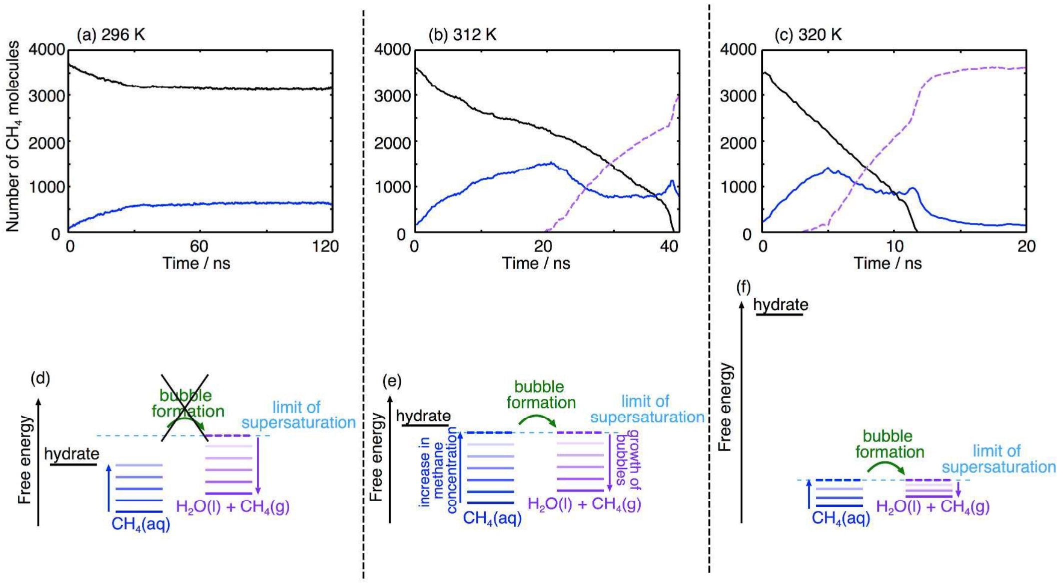

Figure 4 Numbers of methane molecules in the hydrate slab, N_h (black), those dissolved in the aqueous phase, N_a (blue), and those in bubbles, N_b (purple), against time for the pure water system at (a) T = 296 K, (b) 312 K, and (c) 320 K, and the schematics for the hydrate dissociation mechanism at (d) low, (e) medium, and (f) high temperature regions.

We present a schematic representation of the dissociation behavior of methane hydrate at T = 312 K in Figure 4e. The molar free energy of the hydrate phase (black horizontal bar) is higher than that of the final state of the dissociation, i.e., the two-phase coexistence of liquid water and methane gas (the darkest purple solid bar). In the initial stage of the dissociation process, however, the dissociation rate does not depend on the difference in the free energy between these two states. Rather, the dissociation rate is governed by the difference between the free energy of the hydrate phase (black bar) and that of the aqueous methane solution (blue bar). At t = 0, the free energy of the aqueous solution is low because there is no methane in the solution (the darkest blue bar at the bottom). The free energy level of the aqueous solution becomes higher as the concentration of methane in the solution increases due to the positive excess chemical potential of methane in water (this is represented by the blue upward arrow). Because the gap between the black and blue bars in the figure decreases, the dissociation rate decreases with time. This is seen for $0 < t < 20$ in Figure 4b. At $t \sim 20$ ns, the concentration of methane in the aqueous phase reaches the limit of supersaturation, and the first bubble forms as shown in Figure 2. At this moment, the driving force for the dissociation changes from the free energy difference between the solid black bar and the dashed blue bar to that between the solid black bar and the dashed purple bar. The bubbles absorb methane molecules in the aqueous phase and grow rapidly. This results in the decreases in the free energy of the two-phase coexistence of liquid water and methane gas (this is shown by the purple downward arrow). Therefore, the dissociation rate of the hydrate slab increases after the bubble formation.

Figure 4f is a schematic for the dissociation behavior at high temperatures such as $T = 320$ K. The free energy of the hydrate phase is higher for higher temperatures. At $T = 320$ K, it becomes much higher that the free energy level of the aqueous solution at the limit of super saturation (dashed light blue line). In this case, the changes in the free energy levels with time, which are expressed by the blue and purple vertical arrows, are negligible compared with the gap between the black bar and the dashed light blue line. Therefore, bubble formation does not affect the dissociation rate, and the number of methane molecule in the hydrate slab, N_h, linearly decreases with respect to time as shown in Figure 4c. Early MD simulation studies also showed time-independent dissociation rates of gas hydrates.[81-84] These studies examined this high-temperature case.

Figure 4a shows the dissociation behavior at T = 296 K. The dissociation rate decreases with time for $0 < t < 35$ ns. No bubble forms at this temperature within the simulation time of 120 ns. The schematic for this behavior is presented in Figure 4d. The free energy of the aqueous methane solution (blue) increases with time because of the released methane molecules from the hydrate slab. Due to the low temperature, the free energy of the hydrate slab (black) is lower than that of the aqueous methane solution at the concentration of the limit of supersaturation (dashed light blue line). In this case, the increase in the free energy of the aqueous methane solution stops when the level of the blue bar becomes identical to that of the black bar. Therefore, the dissociation of methane hydrate stops without bubble formation.

Experimentally, the dissociation temperature of methane hydrate is 193 K under ambient pressure. The dissociation temperature of the combination of the TIP4P/2005 and OPLS model is lower than the experimental value.[58] Thus, the free energy of the hydrate phase is higher than the final state of the hydrate dissociation, $H_2O(l) + CH_4(g)$, at all the temperatures examined in this study. Nevertheless, the hydrate slab only partially dissociates for $T \leq 300$ K because of the lack of bubble formation as schematically shown in Figure 4d. It was reported that the limit of supersaturation of methane in water decreases with increasing system size.[114] In other words, bubbles form more easily in larger systems. If an MD simulation is performed for a larger system with the same composition ratio, bubble formation and the following hydrate dissociation would occur at temperatures lower than 300 K. It should be noted that the barrier of bubble formation does not become zero even when the system is infinitely large. This indicates that gas hydrates can survive for long period at temperatures higher than the hydrate/liquid/gas three-phase equilibrium temperature in real system if there is no preexistent bubble near the hydrate. The possibility of superheating of gas hydrates due to this mechanism was first proposed by Buffett and Zatsepina in 1999.[115]

In order to evaluate the reproducibility of the observed results, we generate three hydrate structures with different proton arrangements, and compare the dissociation behaviors of them at T = 308 K. Figure 5 presents N_h for the three simulation runs. The three curves almost overlap during the initial 30 ns, where the dissociation rate decreases with time due to the increase in the free energy level of CH_4(aq). This indicates that the effect of the difference in the proton arrangement is insignificant for the dissociation rate in this period. In contrast, the dissociation behaviors for $t > 30$ ns are quite different from each other due to the highly stochastic nature of bubble nucleation. The elapsed times before bubble formation are 60, 50, and 30 ns for runs a, b, and c, respectively. The dissociation rate after the bubble formation in run-a is faster than those in the other two simulation runs because two bubbles form in run-a whereas only one bubble form in run-b and run-c. Figure 5 also shows N_h of three different simulations performed at T = 320 K. Bubble formation does not affect the dissociation rate at the high temperature region. Therefore, the results of the three simulations are almost the same at T = 320 K. The dispersion in the time for complete dissociation mainly arises from the bubble nucleation. However, it is difficult to analyze the dispersion quantitatively because hundreds of trajectories are required to characterize a stochastic nucleation event and huge computational resources are needed to obtain them.[116, 117] This issue is beyond the scope of the present study. Note that the three trajectories exhibit essentially the same behavior. This result ensures that qualitative conclusion on the effects of temperature and TIs, which are the focus of the present study, can be derived from the limited number of trajectories.

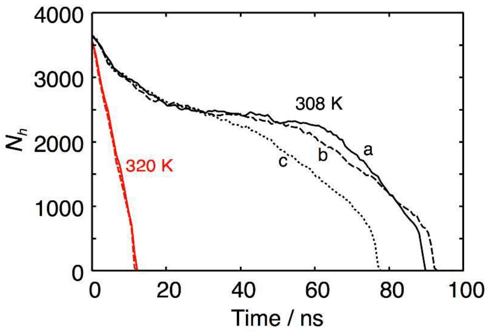

Figure 5 Comparison between three simulations starting from structures with different proton arrangements at T = 308 K (black) and 320 K (red).

We examine the location of bubble formation. The first bubble forms at t = 20 ns in the simulation performed at T = 312 K. Figure 6a presents the distribution function of methane molecules along the z-axis immediately after the bubble formation. It is seen that the dissolved methane molecules are uniformly distributed in the aqueous phase, -73 Å < z < 73 Å. This indicates that the timescale of the release of methane molecules from the hydrate slab is slower than that of the diffusion of methane molecules in water. Due to the uniform distribution, bubble formation can occur anywhere in the aqueous phase. In this simulation, the first bubble incidentally forms at $z \sim 0$ Å. Figure 6b shows the distribution functions at T = 336 K, which is the highest temperature examined in this study. The distribution of dissolved methane molecule is not uniform when the first bubble emerges in the aqueous phase at t = 0.5 ns, because the dissociation of the hydrate slab is quite fast compared to the diffusion of methane in water. Therefore, methane bubbles tend to form in the vicinity of the hydrate surface. The formation of bubbles near the hydrate surface in the high temperature region was also observed in early simulation studies.[89-91]

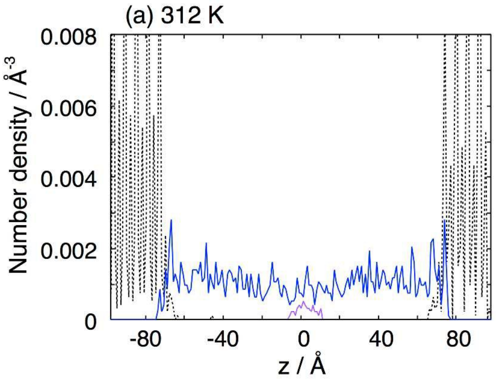

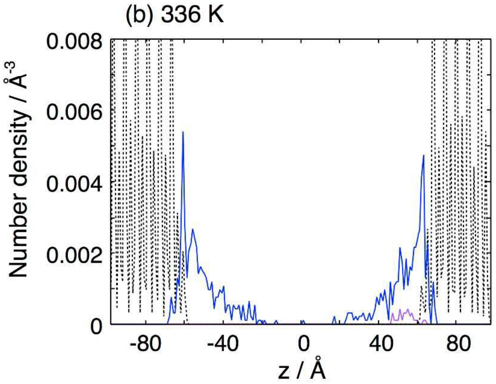

Figure 6 Distribution functions of methane molecules along the *z*-axis immediately after the first bubble formation at (a) T = 312 K and (b) T = 336 K. The black, blue, and purple curves show the distribution functions of methane molecules in the hydrate slab, those dissolved in water, and those in the first bubble, respectively.

In this study, the simulations are performed for a hydrate-rich condition with periodic boundary conditions. It is possible to infer the dissociation mechanism in open water-rich systems, such as a hydrate crystal immersed in a mass of water. In open water-rich systems, the concentration of methane molecules decreases as the distance from the hydrate surface increases, and the distribution of dissolved methane molecules does not become uniform. If the time scale of the release of methane from the hydrate is much slower than that of the diffusion process of methane in water, the hydrate crystal would completely dissociates without bubble formation in open water-rich systems. However, bubble formation is commonly observed in experiments of dissociation of gas hydrates.[118, 119] This fact implies that the diffusion of methane is slow and bubble formation occurs "near" the hydrate (the location of the bubble formation is close to the hydrate on a macroscopic length scale, but there can be a space between the bubble and the hydrate surface on a microscopic scale). Thus, the increase in the dissociation rate due to bubble formation likely occurs also in macroscopic water-rich systems. Once a bubble forms and grows to a certain size, or there is a pre-existent gas phase near the hydrate, the dissociation rate would be dominated by the time scale of transferring methane from the vicinity of the hydrate to the gas phase. The transfer of bubbles themselves may also be important as suggested by Ripmeester et al.[89-91]

It should be noted that we focus on the microscopic intrinsic dissociation kinetics and macroscopic heat transfer effect is eliminated using a strong coupling between the system and thermal reservoir (0.6 ps) in this study. Experimentally, it is difficult to access the microscopic intrinsic rate because the measured rate is more or less affected by macroscopic heat transfer due to the slow agitation rate compared with the timescale of MD simulations.[97] In contrast, it is difficult to treat the macroscopic heat transfer in all-atom MD simulations even with current computational power. We mention that several MD studies on gas hydrates have attempted to include this effect.[62, 67, 89-91]

Effects of thermodynamic inhibitors

In Figure 7a, we compare N_h in pure water (solid black), in the aqueous methanol solution (solid red), and in the NaCl solution (solid green) at *T* = 312 K. It is found that the dissociation in the methanol solution is faster than that in pure water. In contrast, the dissociation in the NaCl solution is slower than that in pure water in the initial ~10 ns.

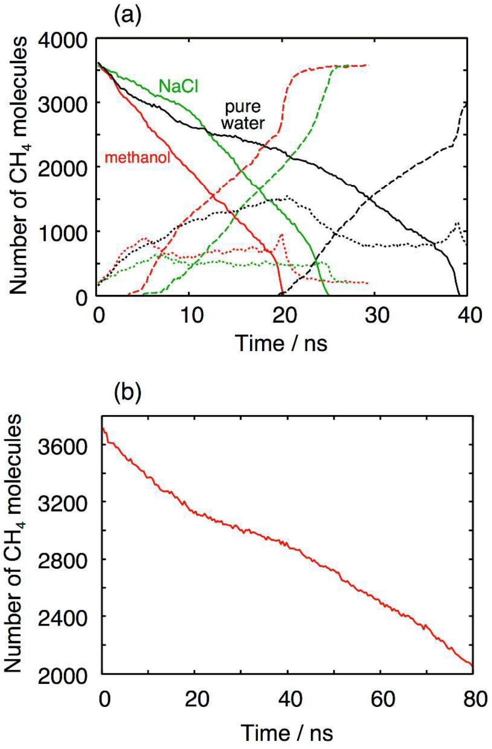

Figure 7 (a) Dissociation behavior of methane hydrate at *T* = 312 K in pure water (black), in the aqueous methanol solution (red), and in the NaCl solution (green). Solid, dotted, and dashed curves show the numbers of methane molecules in the hydrate slab (N_h), those dissolved in the aqueous solution (N_a), and those in bubbles (N_b), respectively. (b) Time evolution of N_h in the methanol solution at *T* = 296 K.

The dissociation rate in the initial stage is increased by methanol whereas it is decreased by NaCl. This is explained from the effects of them on the hydration free energy of methane, G_{hyd}. We calculate the hydration free energy of methane at *T* = 312

K. We find that G_{hyd} in the aqueous methanol solution, 8.9 kJ mol^{-1}, is lower that in pure water, 9.9 kJ mol^{-1}, i.e., the solubility of methane is higher in the methanol solution. This is consistent with experimental results.[120] The lower hydration free energy can be attributed to the stabilization of methane due to the hydrophobic group of methanol. This result indicates that the free energy level of CH_4(aq) is lowered by methanol as schematically shown in Figure 8a. Therefore, the dissociation of methane hydrate in the methanol solution is faster than that in pure water. In contrast, G_{hyd} in the NaCl solution, 15.2 kJ mol^{-1}, is higher than that in pure water. This is also consistent with experimental observation.[121] NaCl increases G_{hyd} because salts have a similar effect on the structure of liquid water as pressurization: the number of voids in liquid water which can accommodate methane molecules is reduced by the presence of ions.[122, 123] Thus, the initial dissociation rate in the NaCl solution is lower than that in pure water.

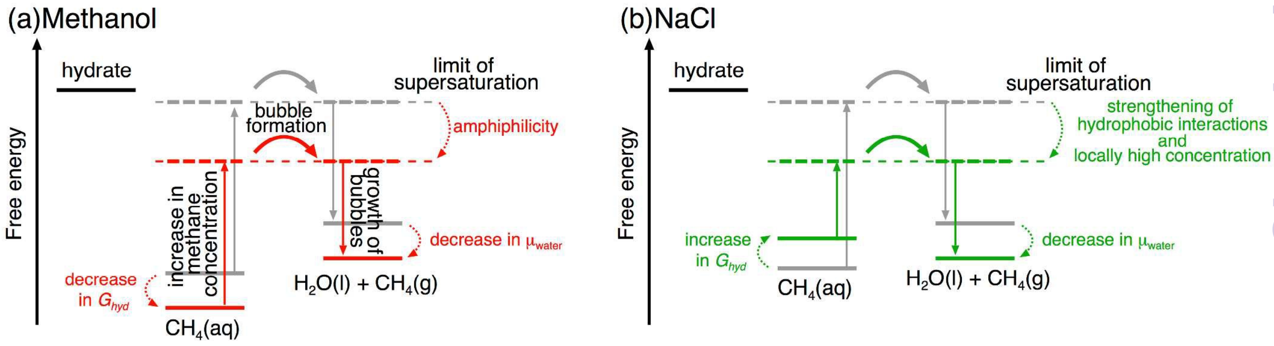

Figure 8 Schematics of the effects of (a) methanol and (b) NaCl on the dissociation mechanism of methane hydrate in aqueous solutions. The free energy levels in pure water are gray, and those in the methanol and NaCl solutions are colored red and green, respectively. The dotted arrows show the effects of the methanol and NaCl whereas the solid arrows represent the changes in the state as the dissociation proceeds.

Figure 7a shows that the number of methane molecules in the aqueous phase, N_a, is

800 when the first bubble forms at t = 4 ns in the methanol solution. In pure water, N_a is 1500 when the first bubble emerges at t = 20 ns. These results indicate that the presence of methanol facilitates the formation of methane bubbles, i.e., methanol lowers the free energy level of the limit of supersaturation (dashed line) as shown in Figure 8a. Methanol also lowers the free energy level of CH_4(aq) and that of H_2O(l) + CH_4(g). As a result, the free energy of the hydrate phase becomes much higher than those of the other states. This is in essence the same as the effect caused by the increase in temperature (Figure 4e → 4f). That is, the linear decrease in N_h against time, which is the characteristic for the dissociation behavior in the high temperature region above 320 K in pure water (Figure 3a), is seen in the methanol solution at T = 312 K (Figure 7a). The nonlinear decrease in N_h is observed in the methanol solution at lower temperatures. Figure 7b presents the time evolution of N_h in the methanol solution at T = 296 K. The first bubble forms at t = 33 ns in this simulation. Figure 7b demonstrates that the dissociation rate increases after this bubble formation. A snapshot of the bubble at t = 33 ns is presented in Figure 9a. This figure displays not only methane molecules but also methanol and water molecules in contact with the bubble. We define that a methanol (water) molecule is in contact with the bubble if the distance between one of methane molecule in the bubble and the CH_3 group of the methanol (oxygen of water) is less than 6 Å (5.5 Å), which is the minimum position of the radial distribution function. The bubble consists of 49 methane molecules, and it is surrounded by 42 methanol molecules and 147 water molecules. The ratio of the number of methanol molecules to that of water molecules, 42/147 = 0.29, is much larger than that for the bulk liquid region, 1/9 = 0.11 (mole fraction of the methanol in the solution is 0.1). Figure 9b shows the radial density functions around the center of mass of the bubble. It is shown

that there is no water molecule inside the bubble of methane, $r < 6$ Å. The concentration of methanol around the bubble, $r \sim 10$ Å, is higher than that in the bulk region of the solution, $r > 15$ Å. The distribution functions of methanol (black and green) suggest that the methyl group points toward the cluster of methane whereas the hydroxyl group points toward the aqueous phase. The amphiphilic character of methanol stabilizes small clusters of methane, and thus bubbles can easily form in the methanol solution.

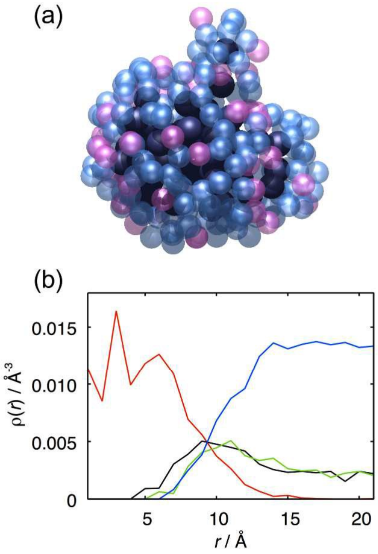

Figure 9 (a) Snapshot of a bubble of methane molecules at $t = 33$ ns in the methanol solution at $T = 296$ K. Methane molecules in the bubble are represented by dark blue spheres. Oxygen atoms in methanol and water molecules in contact with the bubble are shown by magenta and light blue spheres, respectively. (b) Radial density functions around the center of mass of the bubble in the methanol solution at $t = 33$ ns. The red, black, green, and blue curves show the radial density functions of methane molecules in the bubble, CH_3 of methanol, H of the hydroxyl group of methanol, and O of water, respectively. The radial density function of O of water is multiplied by 0.5.

Figure 7a shows that the first bubble forms at t = 20 ns in pure water whereas it forms at t = 5.4 ns in the NaCl solution. Due to the rapid bubble formation, the hydrate dissociation in the NaCl solution finishes much earlier than that in pure water, although the initial dissociation rate is lower in the NaCl solution. The number of dissolved methane molecules in the aqueous phase at the moment of bubble formation in the NaCl solution is 600. This is much smaller than the corresponding result for the pure water system, 1500. This indicates that NaCl also facilitates the bubble formation (Figure 8b). However, the mechanism for the enhancement of bubble formation due to ions is different from the mechanism of methanol. Ghosh et al. calculated the methane-methane potential of mean force in aqueous NaCl solutions.[124] They found that the contact configuration of the methane pair is stabilized by Na^+ and Cl^-. Because of the strengthening of the hydrophobic interactions, bubbles form more easily in NaCl solutions than in pure water.

The distribution of dissolved methane molecules in the NaCl solution is quite different from that in pure water at the same temperature. Figure 10 shows the distribution functions of methane molecules and Cl^- immediately after the first bubble formation at t = 5.4 ns in the NaCl solution at T = 312 K. The concentration of Cl^- near the hydrate surface, $|z| \sim 50$ Å, is lower than that in the bulk region of the solution because water molecules are released from the hydrate slab in the dissociation process. As shown above, the hydration free energy of methane in the NaCl solution is higher than that in pure water. As a result, the methane molecules released from the hydrate prefer to stay in the ion-poor region near the hydrate surface. The emergence of the locally high concentration near the surface also assists the rapid bubble formation in the

NaCl solution because methane molecules can easily form a contact pair in this region. The first bubble forms at z = -50 Å. The bubble keeps in contact with the hydrate surface during the dissociation process, because not only each methane molecule but also a cluster of them do not favor the ion-rich region. A similar behavior is observed at other temperatures in the NaCl solution,[94] whereas no bubble contacts with the hydrate surface in pure water and in the methanol solution.

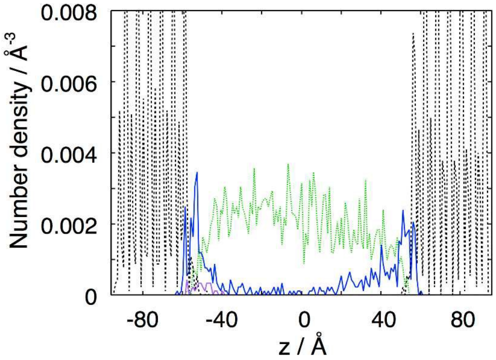

Figure 10 Distribution functions of methane molecules along the z-axis immediately after the first bubble formation at T = 312 K in the aqueous NaCl solution. The black, blue, and purple curves show the distribution functions of methane molecules in the hydrate slab, those dissolved in water, and those in the first bubble. The green curve is the distribution function of Cl^-. That of Na^+ is not shown because it is similar to the distribution function of Cl^-.

Conclusions

We have investigated the dissociation of methane hydrate in pure water, in an aqueous methanol solution, and in an aqueous NaCl solution. The dissociation rate of the hydrate initially decreases with time because of the increase in the free energy of the aqueous phase due to methane molecules released from the hydrate. The dissociation rate of this stage is increased by methanol whereas decreased by NaCl. This behavior is explained from the opposite effects of methanol and NaCl on the hydration free energy of methane, i.e., methanol stabilizes methane molecules in the aqueous solution whereas NaCl destabilizes them. The dissociation rate of methane hydrate increases after formation of methane bubbles because the bubbles absorb surrounding methane molecules. It is found that both methanol and NaCl facilitate the bubble formation, but the mechanisms of them are different from each other.

We have demonstrated significant effects of the two TIs on the dissociation kinetics of methane hydrate. Various molecules, including TIs, dissolved in the aqueous phase would affect the growth mechanism of clathrate hydrates as well as the dissociation process. However, there have been a limited number of simulation studies on the hydrate growth with additives.[57, 125] It is known that some water-soluble polymers act as kinetic hydrate inhibitors (KHIs), which adsorb on the hydrate surface and significantly retard the crystal growth.[5, 6] Uses of KHIs combining with TIs have been proposed to prevent formation of clathrate hydrates efficiently in gas and oil pipelines.[5] It was reported that the performance of a KHI can be altered by methanol and NaCl.[126] Recently, we showed the microscopic mechanism of the adsorption of KHIs on the hydrate surface by using MD simulations.[127] However, the details of the inhibition process and effects of additives such as methanol are still unclear. MD simulations would provide a wealth of information on the mechanism of the inhibition of hydrate formation.

Acknowledgements

The present work was supported by a Grant-in-Aid by JSPS and by HPCI Strategic

Programs for Innovative Research (SPIRE) and Computational Materials Science Initiative (CMSI), MEXT, Japan. Calculations were performed on the K computer at the RIKEN Advanced Institute for Computational Science (Project ID: hp140216). A part of calculations was carried out at Research Center for Computational Science, Okazaki, Japan.

References

1. E. D. Sloan and C. A. Koh, *Clathrate Hydrates of Natural Gases*, CPC Press, Boca Raton, 2008.
2. K. A. Kvenvolden, *Ann. N.Y. Acad. Sci.*, 2000, **912**, 17-22.
3. E. D. Sloan, *Nature*, 2003, **426**, 353-359.
4. R. Boswell, *J. Pet. Sci. Eng.*, 2007, **56**, 9-13.
5. M. A. Kelland, *Energy Fuels*, 2006, **20**, 825-847.
6. A. Perrin, O. M. Musa and J. W. Steed, *Chem. Soc. Rev.*, 2013, **42**, 1996-2015.
7. S.-P. Kang and H. Lee, *Environ. Sci. Technol.*, 2000, **34**, 4397-4400.
8. P. Linga, R. Kumar and P. Englezos, *J. Hazard. Mater.*, 2007, **149**, 625-629.
9. W. L. Mao, H.-k. Mao, A. F. Goncharov, V. V. Struzhkin, Q. Guo, J. Hu, J. Shu, R. J. Hemley, M. Somayazulu and Y. Zhao, *Science*, 2002, **297**, 2247-2249.
10. W. L. Mao and H. K. Mao, *Proc. Natl. Acad. Sci. U.S.A.*, 2004, **101**, 708-710.
11. L. J. Florusse, C. J. Peters, J. Schoonman, K. C. Hester, C. A. Koh, S. F. Dec, K. N. Marsh and E. D. Sloan, *Science*, 2004, **306**, 469-471.
12. V. V. Struzhkin, B. Militzer, W. L. Mao, H. K. Mao and R. J. Hemley, *Chem. Rev.*, 2007, **107**, 4133-4151.
13. N. J. English and J. M. D. MacElroy, *Chem. Eng. Sci.*, 2015, **121**, 133-156.
14. H. Tanaka and K. Kiyohara, *J. Chem. Phys.*, 1993, **98**, 4098-4109.
15. H. Tanaka and K. Kiyohara, *J. Chem. Phys.*, 1993, **98**, 8110-8118.
16. K. Koga, H. Tanaka and K. Nakanishi, *J. Chem. Phys.*, 1994, **101**, 3127-3134.
17. K. Katsumasa, K. Koga and H. Tanaka, *J. Chem. Phys.*, 2007, **127**, 044509.
18. T. Nakayama, K. Koga and H. Tanaka, *J. Chem. Phys.*, 2009, **131**, 214506.
19. A. Wallqvist, *J. Chem. Phys.*, 1992, **96**, 5377-5382.
20. R. E. Westacott and P. M. Rodger, *J. Chem. Soc., Faraday Trans.*, 1998, **94**, 3421-3426.
21. H. Docherty, A. Galindo, C. Vega and E. Sanz, *J. Chem. Phys.*, 2006, **125**, 074510.
22. T. Miyoshi, M. Imai, R. Ohmura and K. Yasuoka, *J. Chem. Phys.*, 2007, **126**, 234506.
23. E. A. Mastny, C. A. Miller and J. J. de Pablo, *J. Chem. Phys.*, 2008, **129**, 034701.
24. M. M. Conde, C. Vega, G. A. Tribello and B. Slater, *J. Chem. Phys.*, 2009, **131**, 034510.
25. L. Jensen, K. Thomsen, N. von Solms, S. Wierzchowski, M. R. Walsh, C. A. Koh, E. D. Sloan, D. T. Wu and A. K. Sum, *J. Phys. Chem. B*, 2010, **114**, 5775-5782.
26. J. S. Tse, M. L. Klein and I. R. McDonald, *J. Phys. Chem.*, 1983, **87**, 4198-4203.
27. P. M. Rodger, T. R. Forester and W. Smith, *Fluid Phase Equilib.*, 1996, **116**, 326-332.
28. V. Chihaia, S. Adams and W. F. Kuhs, *Chem. Phys.*, 2005, **317**, 208-225.

29. H. Jiang, K. D. Jordan and C. E. Taylor, *J. Phys. Chem. B*, 2007, **111**, 6486-6492.
30. S. Alavi, J. A. Ripmeester and D. D. Klug, *J. Chem. Phys.*, 2005, **123**, 24507.
31. S. Alavi, K. Shin and J. A. Ripmeester, *J. Chem. Eng. Data*, 2015, **60**, 389-397.
32. G.-J. Guo and P. M. Rodger, *J. Phys. Chem. B*, 2013, **117**, 6498-6504.
33. C. Moon, P. C. Taylor and P. M. Rodger, *J. Am. Chem. Soc.*, 2003, **125**, 4706-4707.
34. R. W. Hawtin, D. Quigley and P. M. Rodger, *Phys. Chem. Chem. Phys.*, 2008, **10**, 4853-4864.
35. J. Vatamanu and P. G. Kusalik, *J. Phys. Chem. B*, 2006, **110**, 15896-15904.
36. J. Vatamanu and P. G. Kusalik, *J. Am. Chem. Soc.*, 2006, **128**, 15588-15589.
37. J. Vatamanu and P. G. Kusalik, *J. Phys. Chem. B*, 2008, **112**, 2399-2404.
38. J. Vatamanu and P. G. Kusalik, *Phys. Chem. Chem. Phys.*, 2010, **12**, 15065-15072.
39. S. Liang and P. G. Kusalik, *J. Phys. Chem. B*, 2010, **114**, 9563-9571.
40. S. Liang and P. G. Kusalik, *Chemical Science*, 2011, **2**, 1286.
41. P. Pirzadeh and P. G. Kusalik, *J. Am. Chem. Soc.*, 2013, **135**, 7278-7287.
42. M. R. Walsh, C. A. Koh, E. D. Sloan, A. K. Sum and D. T. Wu, *Science*, 2009, **326**, 1095-1098.
43. M. R. Walsh, G. T. Beckham, C. A. Koh, E. D. Sloan, D. T. Wu and A. K. Sum, *J. Phys. Chem. C*, 2011, **115**, 21241-21248.
44. L. C. Jacobson, W. Hujo and V. Molinero, *J. Am. Chem. Soc.*, 2010, **132**, 11806-11811.
45. L. C. Jacobson, W. Hujo and V. Molinero, *J. Phys. Chem. B*, 2010, **114**, 13796-13807.
46. A. H. Nguyen, L. C. Jacobson and V. Molinero, *J. Phys. Chem. C*, 2012, **116**, 19828-19838.
47. B. C. Knott, V. Molinero, M. F. Doherty and B. Peters, *J. Am. Chem. Soc.*, 2012, **134**, 19544-19547.
48. R. Radhakrishnan and B. L. Trout, *J. Chem. Phys.*, 2002, **117**, 1786-1796.
49. S. Sarupria and P. G. Debenedetti, *J. Phys. Chem. Lett.*, 2012, **3**, 2942-2947.
50. N. J. English and J. M. D. MacElroy, *J. Chem. Phys.*, 2004, **120**, 10247-10256.
51. N. J. English, M. Lauricella and S. Meloni, *J. Chem. Phys.*, 2014, **140**, 204714.
52. F. Jiménez-Ángeles and A. Firoozabadi, *J. Phys. Chem. C*, 2014, **118**, 11310-11318.
53. M. Lauricella, S. Meloni, N. J. English, B. Peters and G. Ciccotti, *J. Phys. Chem. C*, 2014, **118**, 22847-22857.
54. H. Nada, *J. Phys. Chem. B*, 2006, **110**, 16526-16534.
55. H. Nada, *J. Phys. Chem. B*, 2009, **113**, 4790-4798.
56. Y. T. Tung, L. J. Chen, Y. P. Chen and S. T. Lin, *J. Phys. Chem. B*, 2010, **114**, 10804-10813.
57. Y.-T. Tung, L.-J. Chen, Y.-P. Chen and S.-T. Lin, *J. Phys. Chem. B*, 2012, **116**,

14115-14125.

58. M. M. Conde and C. Vega, *J. Chem. Phys.*, 2010, **133**, 064507.

59. V. K. Michalis, J. Costandy, I. N. Tsimpanogiannis, A. K. Stubos and I. G. Economou, *J. Chem. Phys.*, 2015, **142**, 044501.

60. J.-Y. Wu, L.-J. Chen, Y.-P. Chen and S.-T. Lin, *J. Phys. Chem. C*, 2015, **119**, 1400-1409.

61. S. Liang, D. Rozmanov and P. G. Kusalik, *Phys. Chem. Chem. Phys.*, 2011, **13**, 19856-19864.

62. S. Liang and P. G. Kusalik, *J. Phys. Chem. B*, 2013, **117**, 1403-1410.

63. J. Bai and X. C. Zeng, *Proc. Natl. Acad. Sci. U.S.A.*, 2012, **109**, 21240-21245.

64. J. Bai, C. A. Angell and X. C. Zeng, *Proc. Natl. Acad. Sci. U.S.A.*, 2010, **107**, 5718-5722.

65. W.-H. Zhao, L. Wang, J. Bai, L.-F. Yuan, J. Yang and X. C. Zeng, *Acc. Chem. Res.*, 2014, **47**, 2505-2513.

66. A. Phan, D. R. Cole and A. Striolo, *J. Phys. Chem. C*, 2014, **118**, 4860-4868.

67. Z. Zhang, M. R. Walsh and G. J. Guo, *Phys. Chem. Chem. Phys.*, 2015, **17**, 8870-8876.

68. S. Alavi and J. A. Ripmeester, *Angew. Chem.*, 2007, **119**, 6214-6217.

69. T. J. Frankcombe and G.-J. Kroes, *J. Phys. Chem. C*, 2007, **111**, 13044-13052.

70. B. Peters, N. E. R. Zimmermann, G. T. Beckham, J. W. Tester and B. L. Trout, *J. Am. Chem. Soc.*, 2008, **130**, 17342-17350.

71. H. Cao, N. J. English and J. M. MacElroy, *J. Chem. Phys.*, 2013, **138**, 094507.

72. S. Liang and P. G. Kusalik, *J. Am. Chem. Soc.*, 2011, **133**, 1870-1876.

73. P. D. Gorman, N. J. English and J. M. MacElroy, *J. Chem. Phys.*, 2012, **136**, 044506.

74. R. Inoue, H. Tanaka and K. Nakanishi, *J. Chem. Phys.*, 1996, **104**, 9569-9577.

75. N. J. English and J. S. Tse, *Comput. Mater. Sci.*, 2010, **49**, S176-S180.

76. L. A. Baez and P. Clancy, *Ann. N.Y. Acad. Sci.*, 1994, **715**, 177-186.

77. P. M. Rodger, *Ann. N.Y. Acad. Sci.*, 2000, **912**, 474-482.

78. K. Yasuoka and S. Murakoshi, *Ann. N.Y. Acad. Sci.*, 2000, **912**, 678-684.

79. J. S. Tse and D. D. Klug, *J. Supramol. Chem.*, 2002, **2**, 467-472.

80. B. Kvamme, T. Kuznetsova and K. Aasoldsen, *J. Mol. Graphics Modell.*, 2005, **23**, 524-536.

81. N. J. English, J. K. Johnson and C. E. Taylor, *J. Chem. Phys.*, 2005, **123**, 244503.

82. N. J. English and G. M. Phelan, *J. Chem. Phys.*, 2009, **131**, 074704.

83. E. M. Myshakin, H. Jiang, R. P. Warzinski and K. D. Jordan, *J. Phys. Chem. A*, 2009, **113**, 1913-1921.

84. S. Sarupria and P. G. Debenedetti, *J. Phys. Chem. A*, 2011, **115**, 6102-6111.
85. G. S. Smirnov and V. V. Stegailov, *J. Chem. Phys.*, 2012, **136**, 044523.
86. Y. Liu, J. J. Zhao and J. C. Xu, *Comput. Theor. Chem.*, 2012, **991**, 165-173.
87. M. Uddin and D. Coombe, *J. Phys. Chem. A*, 2014, **118**, 1971-1988.
88. S. Liang, L. Yi and D. Liang, *J. Phys. Chem. C*, 2014, **118**, 28542-28547.
89. S. Alavi and J. A. Ripmeester, *J. Chem. Phys.*, 2010, **132**, 144703.
90. S. A. Bagherzadeh, P. Englezos, S. Alavi and J. A. Ripmeester, *J. Chem. Thermodyn.*, 2012, **44**, 13-19.
91. S. A. Bagherzadeh, S. Alavi, J. A. Ripmeester and P. Egnglezos, *Fluid Phase Equilib.*, 2013, **358**, 114-120.
92. S. A. Bagherzadeh, P. Englezos, S. Alavi and J. A. Ripmeester, *J. Phys. Chem. B*, 2012, **116**, 3188-3197.
93. T. Yagasaki, M. Matsumoto, Y. Andoh, S. Okazaki and H. Tanaka, *J. Phys. Chem. B*, 2014, **118**, 1900-1906.
94. T. Yagasaki, M. Matsumoto, Y. Andoh, S. Okazaki and H. Tanaka, *J. Phys. Chem. B*, 2014, **118**, 11797-11804.
95. S. Das, V. S. Baghel, S. Roy and R. Kumar, *Phys. Chem. Chem. Phys.*, 2015, **17**, 9509-9518.
96. H. C. Kim, P. R. Bishnoi, R. A. Heidemann and S. S. H. Rizvi, *Chem. Eng. Sci.*, 1987, **42**, 1645-1653.
97. M. Clarke and P. R. Bishnoi, *Can. J. Chem. Eng.*, 2001, **79**, 143-147.
98. R. Kirkpatrick, *Am. Mineral.*, 1975, **60**, 798-814.
99. B. Hess, C. Kutzner, D. van der Spoel and E. Lindahl, *J. Chem. Theory Comput.*, 2008, **4**, 435-447.
100. D. Van der Spoel, E. Lindahl, B. Hess, G. Groenhof, A. E. Mark and H. J. C. Berendsen, *J. Comput. Chem.*, 2005, **26**, 1701-1718.
101. T. Darden, D. York and L. Pedersen, *J. Chem. Phys.*, 1993, **98**, 10089-10092.
102. U. Essmann, L. Perera, M. L. Berkowitz, T. Darden, H. Lee and L. G. Pedersen, *J. Chem. Phys.*, 1995, **103**, 8577-8593.
103. J. L. F. Abascal and C. Vega, *J. Chem. Phys.*, 2005, **123**, 234505.
104. W. L. Jorgensen, J. D. Madura and C. J. Swenson, *J. Am. Chem. Soc.*, 1984, **106**, 6638-6646.
105. W. L. Jorgensen, *J. Phys. Chem.*, 1986, **90**, 1276-1284.
106. D. E. Smith and L. X. Dang, *J. Chem. Phys.*, 1994, **100**, 3757-3766.
107. S. Nosé and M. L. Klein, *Mol. Phys.*, 1983, **50**, 1055-1076.
108. M. Parrinello and A. Rahman, *J. Appl. Phys.*, 1981, **52**, 7182-7190.

109. W. G. Hoover, *Phys. Rev. A*, 1985, **31**, 1695-1697.

110. S. Nosé, *Mol. Phys.*, 1984, **52**, 255-268.

111. T. C. Beutler, A. E. Mark, R. C. van Schaik, P. R. Gerber and W. F. van Gunsteren, *Chem. Phys. Lett.*, 1994, **222**, 529-539.

112. C. H. Bennett, *J. Comput. Phys.*, 1976, **22**, 245-268.

113. R. García Fernández, J. L. F. Abascal and C. Vega, *J. Chem. Phys.*, 2006, **124**, 144506.

114. J. Wedekind, D. Reguera and R. Strey, *J. Chem. Phys.*, 2006, **125**, 214505.

115. B. A. Buffett and O. Y. Zatsepina, *Geophys. Res. Lett.*, 1999, **26**, 2981-2984.

116. O. Galkin and P. G. Vekilov, *J. Phys. Chem. B*, 1999, **103**, 10965-10971.

117. D. Knezic, J. Zaccaro and A. S. Myerson, *J. Phys. Chem. B*, 2004, **108**, 10672-10677.

118. C. K. Paull, P. G. Brewer, W. Ussler, E. T. Peltzer, G. Rehder and D. Clague, *Geo-Marine Letters*, 2002, **22**, 198-203.

119. D. Katsuki, R. Ohmura, T. Ebinuma and H. Narita, *J. Appl. Phys.*, 2008, **104**, 083514.

120. A. Ben-Naim, *The Journal of Physical Chemistry*, 1967, **71**, 4002-4007.

121. Z. Duan and S. Mao, *Geochim. Cosmochim. Acta*, 2006, **70**, 3369-3386.

122. Z. Duan, N. Møller, J. Greenberg and J. H. Weare, *Geochim. Cosmochim. Acta*, 1992, **56**, 1451-1460.

123. R. Mancinelli, A. Botti, F. Bruni, M. A. Ricci and A. K. Soper, *Phys. Chem. Chem. Phys.*, 2007, **9**, 2959-2967.

124. T. Ghosh, A. Kalra and S. Garde, *J. Phys. Chem. B*, 2005, **109**, 642-651.

125. C. Moon, R. W. Hawtin and P. M. Rodger, *Faraday Discuss.*, 2007, **136**, 367-382.

126. E. D. Sloan, S. Subramanian, P. N. Matthews, J. P. Lederhos and A. A. Khokhar, *Ind. Eng. Chem. Res.*, 1998, **37**, 3124-3132.

127. T. Yagasaki, M. Matsumoto and H. Tanaka, *J. Am. Chem. Soc.*, 2015, **137**, 12079-12085.

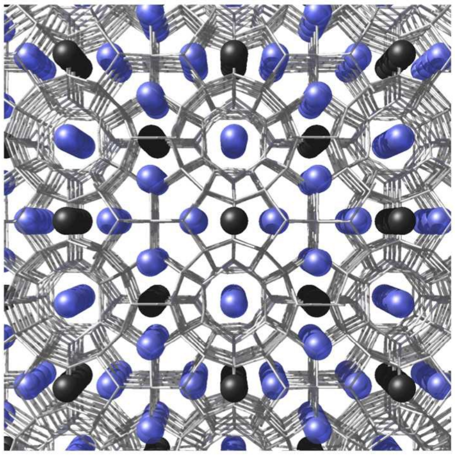

Structure I

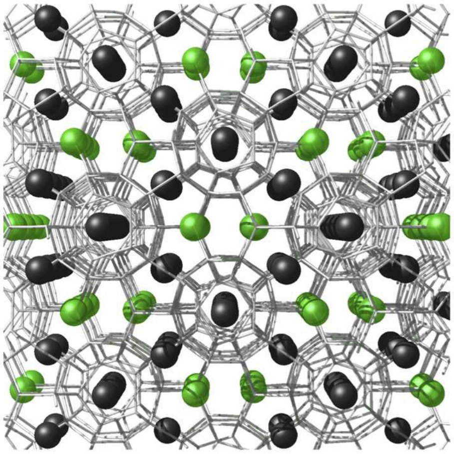

Structure II

(a) 0 ns

(b) 10 ns

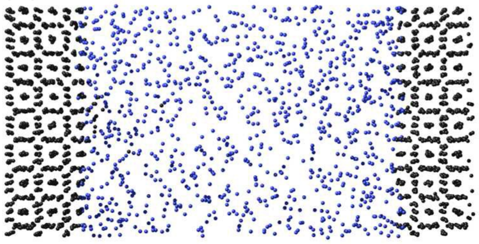

(c) 20 ns

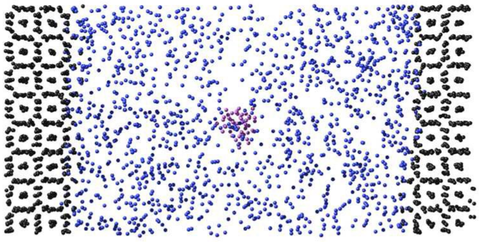

(d) 30 ns

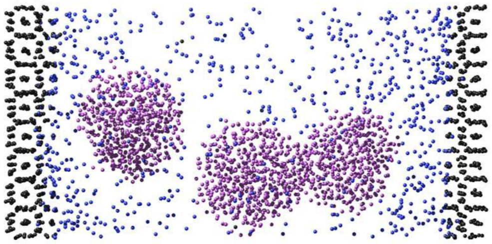

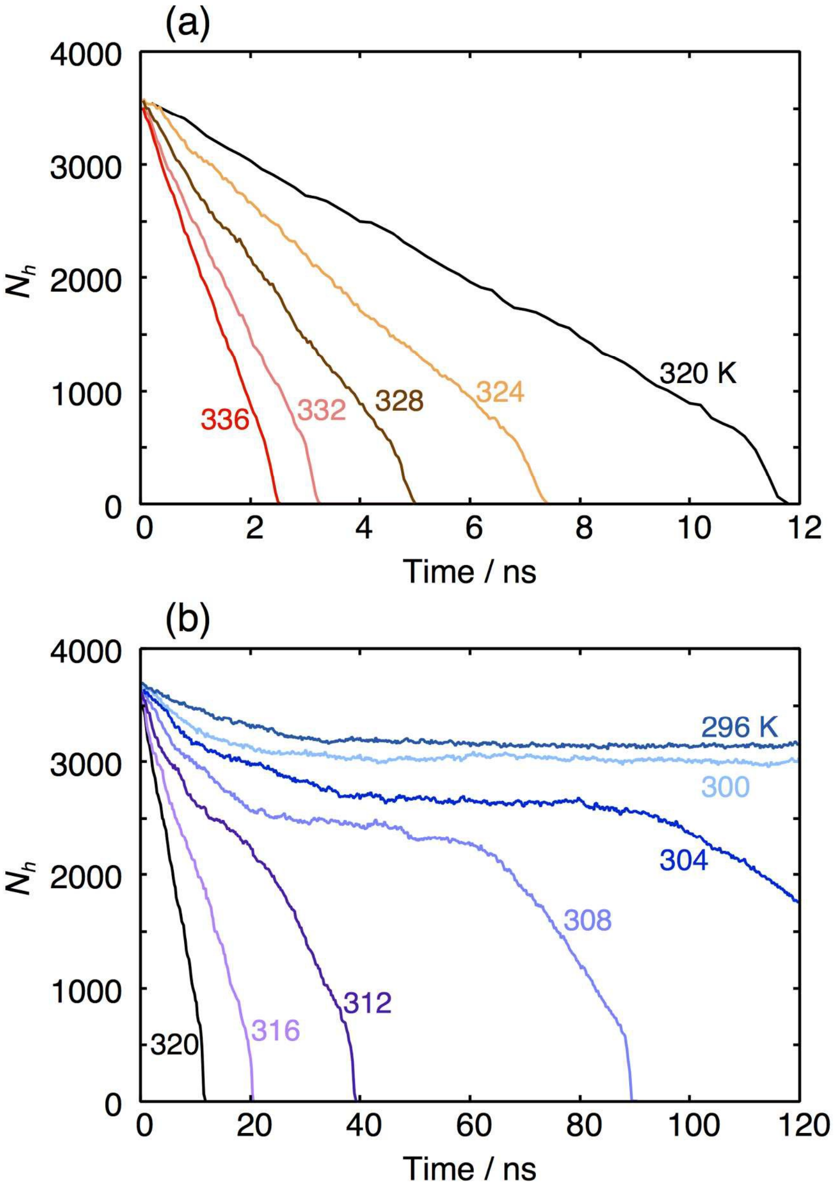
(a)
4000
3000
2000
1000
0
N_h
0
2
4
6
8
10
12
Time / ns
320 K
324
328
332
336
(b)
4000
3000
2000
1000
0
N_h
0
20
40
60
80
100
120
Time / ns
296 K
300
304
308
312
316
320

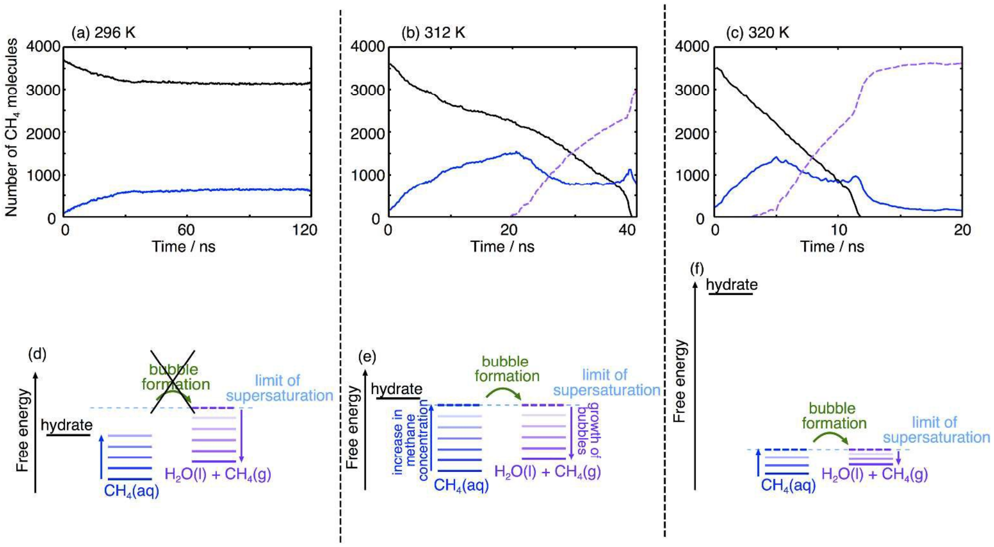
(a) 296 K
(b) 312 K
(c) 320 K
Number of CH_4 molecules
4000
3000
2000
1000
0
0
60
120
20
40
10
Time / ns
(d)
(e)
(f)
Free energy
hydrate
bubble formation
limit of supersaturation
CH_4(aq)
H_2O(l) + CH_4(g)
increase in methane concentration
growth of bubbles

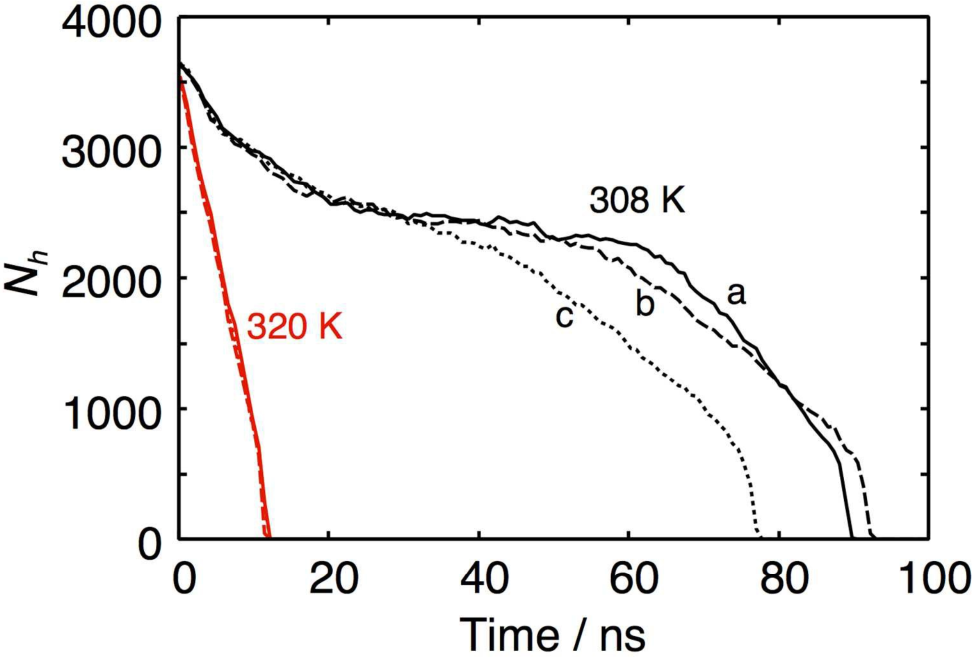
4000
3000
2000
1000
0
N_h
0
20
40
60
80
100
Time / ns
308 K
320 K
a
b
c

(a) 312 K

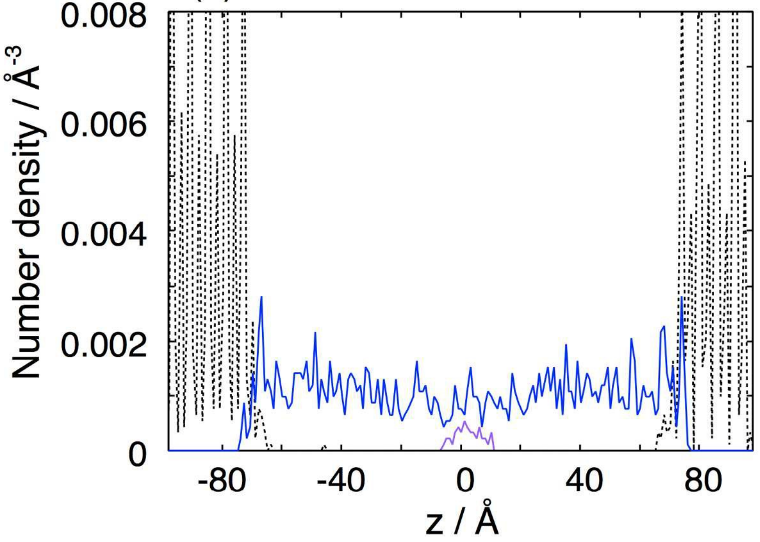
0.008
0.006
0.004
0.002
0
Number density / Å^{-3}
-80
-40
0
40
80
z / Å

(b) 336 K

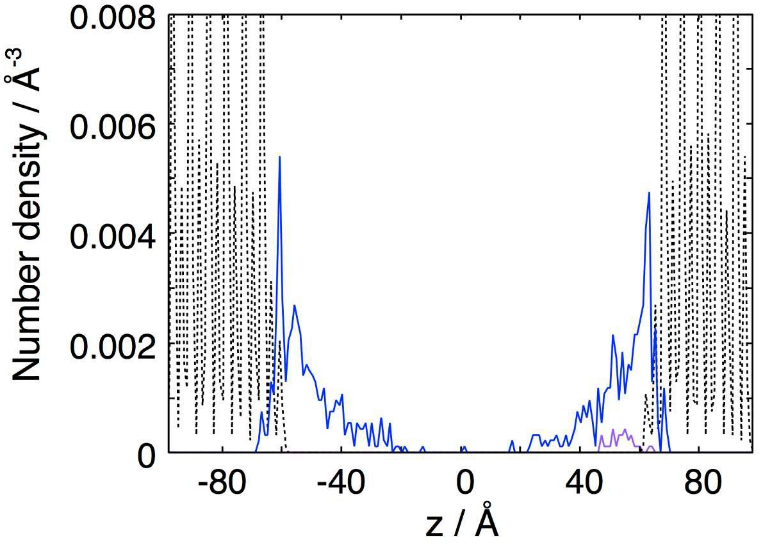
0.008
0.006
0.004
0.002
0
Number density / Å^{-3}
-80
-40
0
40
80
z / Å

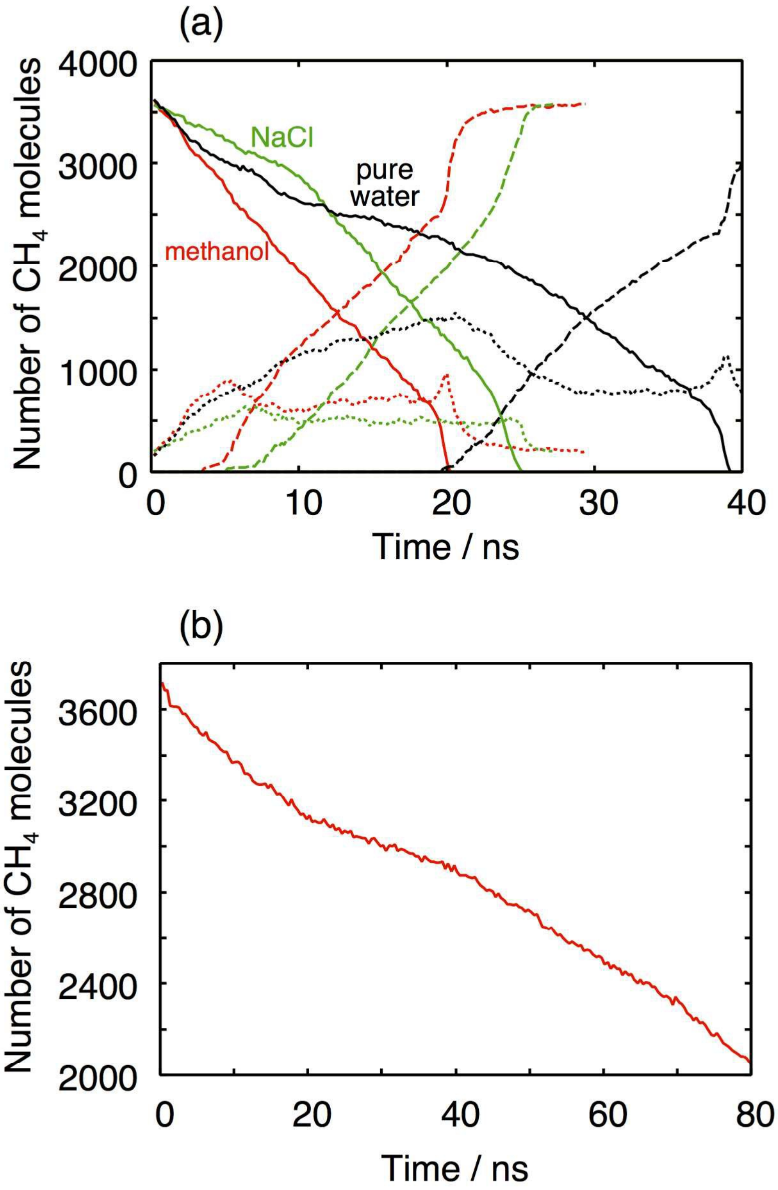
(a)
Number of CH4 molecules
4000
3000
2000
1000
0
0
10
20
30
40
Time / ns
NaCl
pure water
methanol
(b)
Number of CH4 molecules
3600
3200
2800
2400
2000
0
20
40
60
80
Time / ns

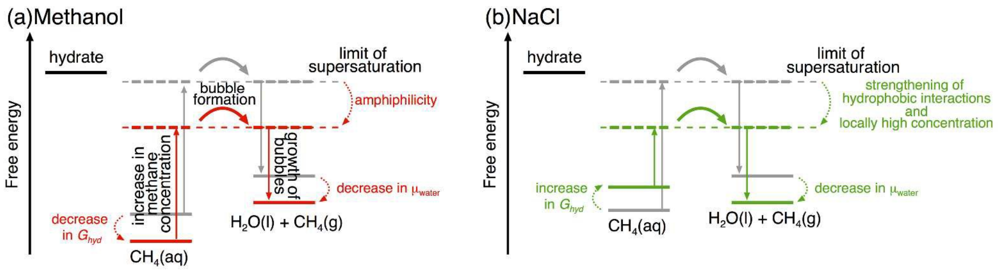
(a)Methanol
Free energy
hydrate
limit of supersaturation
bubble formation
amphiphilicity
increase in methane concentration
growth of bubbles
decrease in μ_{water}
decrease in G_{hyd}
CH_4(aq)
H_2O(l) + CH_4(g)
(b)NaCl
Free energy
hydrate
limit of supersaturation
strengthening of hydrophobic interactions and locally high concentration
increase in G_{hyd}
decrease in μ_{water}
CH_4(aq)
H_2O(l) + CH_4(g)

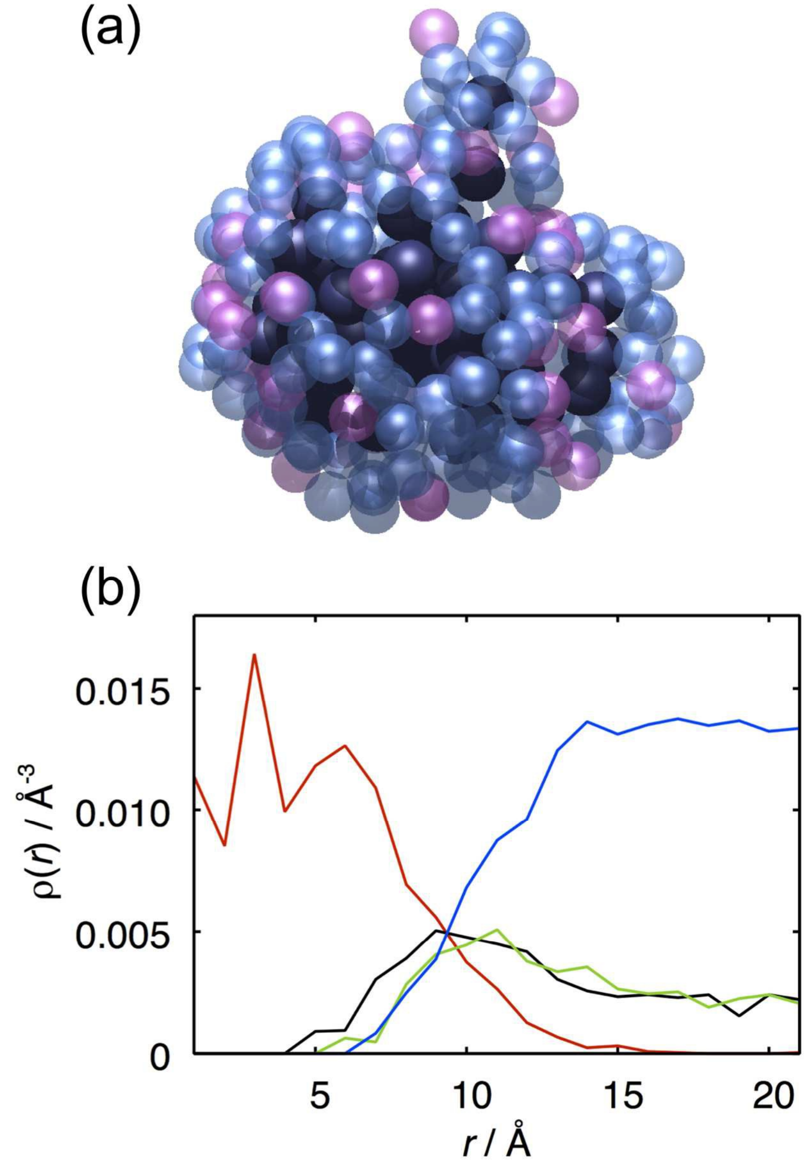
(a)
(b)
0.015
0.010
0.005
0
ρ(r) / Å^{-3}
5
10
15
20
r / Å

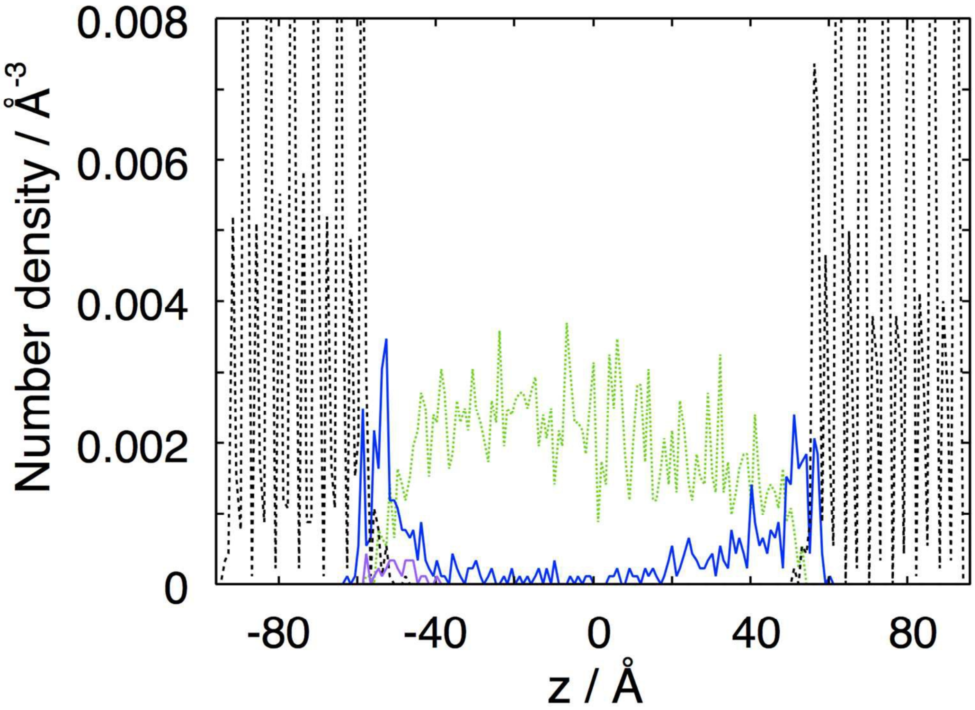
Number density / Å^{-3}
0.008
0.006
0.004
0.002
0
-80
-40
0
40
80
z / Å